AICAR transformylase/IMP cyclohydrolase (ATIC) is essential for *de novo* purine biosynthesis and infection by *Cryptococcus neoformans*

Received for publication, April 25, 2022, and in revised form, August 25, 2022 Published, Papers in Press, September 5, 2022,
https://doi.org/10.1016/j.jbc.2022.102453

Maha S. I. Wizrah[1,2], Sheena M. H. Chua[1,2], Zhenyao Luo[2,3], Mohammad K. Manik[1,2,3], Mengqi Pan[1,2,3], Jessica M. L. Whyte[1,2], Avril A. B. Robertson[1,2,3], Ulrike Kappler[1,2], Bostjan Kobe[1,2,3], and James A. Fraser[1,2,*]

From the [1]Australian Infectious Diseases Research Centre, [2]School of Chemistry & Molecular Biosciences, and [3]Institute for Molecular Bioscience, University of Queensland, St Lucia, Queensland, Australia

Edited by Joseph Jez

The fungal pathogen *Cryptococcus neoformans* is a leading cause of meningoencephalitis in the immunocompromised. As current antifungal treatments are toxic to the host, costly, limited in their efficacy, and associated with drug resistance, there is an urgent need to identify vulnerabilities in fungal physiology to accelerate antifungal discovery efforts. Rational drug design was pioneered in *de novo* purine biosynthesis as the end products of the pathway, ATP and GTP, are essential for replication, transcription, and energy metabolism, and the same rationale applies when considering the pathway as an antifungal target. Here, we describe the identification and characterization of *C. neoformans* 5-aminoimidazole-4-carboxamide ribonucleotide (AICAR) transformylase/5′-inosine monophosphate cyclohydrolase (ATIC), a bifunctional enzyme that catalyzes the final two enzymatic steps in the formation of the first purine base inosine monophosphate. We demonstrate that mutants lacking the ATIC-encoding *ADE16* gene are adenine and histidine auxotrophs that are unable to establish an infection in a murine model of virulence. In addition, our assays employing recombinantly expressed and purified *C. neoformans* ATIC enzyme revealed K_m values for its substrates AICAR and 5-formyl-AICAR are 8-fold and 20-fold higher, respectively, than in the human ortholog. Subsequently, we performed crystallographic studies that enabled the determination of the first fungal ATIC protein structure, revealing a key serine-to-tyrosine substitution in the active site, which has the potential to assist the design of fungus-specific inhibitors. Overall, our results validate ATIC as a promising antifungal drug target.

Fungal infections in humans are notoriously difficult to treat, as the animal and fungal kingdoms share many of the same key biological pathways (1). Pharmaceutical agents used to combat a fungal infection often exhibit significant toxicity to the human host, making treatment difficult (2). Overuse, coupled with incorrect dosing, of the few available antifungals can also lead to drug resistance and recurrent infections (3, 4). Combined with the fact that the past 2 decades have seen limited progress in antifungal drug development, the identification of novel fungal drug targets is a high priority.

Cryptococcus neoformans is among the human fungal pathogens whose infections are challenging to address with available antifungal regimens (5). This basidiomycete yeast can be found in a range of environmental niches, particularly in pigeon excreta and soils (6–8). Infection occurs through the inhalation of fungal cells from the environment, establishing a pulmonary infection in the lungs before dissemination which, because of its remarkable tropism for the central nervous system, often causes meningoencephalitis (9, 10). Globally, approximately a quarter of a million cases each year of cryptococcal meningoencephalitis are recorded, resulting in over 180,000 deaths (72% mortality), with most occurring in regions with a high rate of HIV/AIDS such as sub-Saharan Africa (11).

The pigeon guano in which *C. neoformans* is often found is purine rich, a stark contrast with the purine-poor human host. In the environment, *C. neoformans* can therefore often obtain purines *via* a salvage pathway, but in the infected host, it must rely on *de novo* biosynthesis (12). The purines acquired or created are necessary for processes ranging from DNA and RNA synthesis to energy metabolism and other cellular functions, including translation and signal transduction (13–15).

The canonical *de novo* purine biosynthetic pathway consists of 11 enzymatic steps that convert 5-phosphoribosyl-1-pyrophosphate to the first purine, 5'-inosine monophosphate (IMP), which is then used in the synthesis of AMP and GMP (16). Across the different kingdoms of life, the intermediates in the pathway remain the same, but this is not true for the proteins responsible. A good example of this are the final two steps to produce IMP: 5-aminoimidazole-4-carboxamide ribonucleotide (AICAR) transformylase (Enzyme Commission no.: 2.1.2.3), which converts AICAR to phosphoribosylformamidocarboxamide (FAICAR), and IMP cyclohydrolase (Enzyme Commission no.: 3.5.4.10), which converts FAICAR to IMP (Fig. 1*A*) (17, 18).

In most archaea, the formate-dependent AICAR transformylase PurP generates formyl phosphate that supplies the formyl group for ligation to AICAR to form FAICAR. In some

* For correspondence: James A. Fraser, j.fraser1@uq.edu.au.

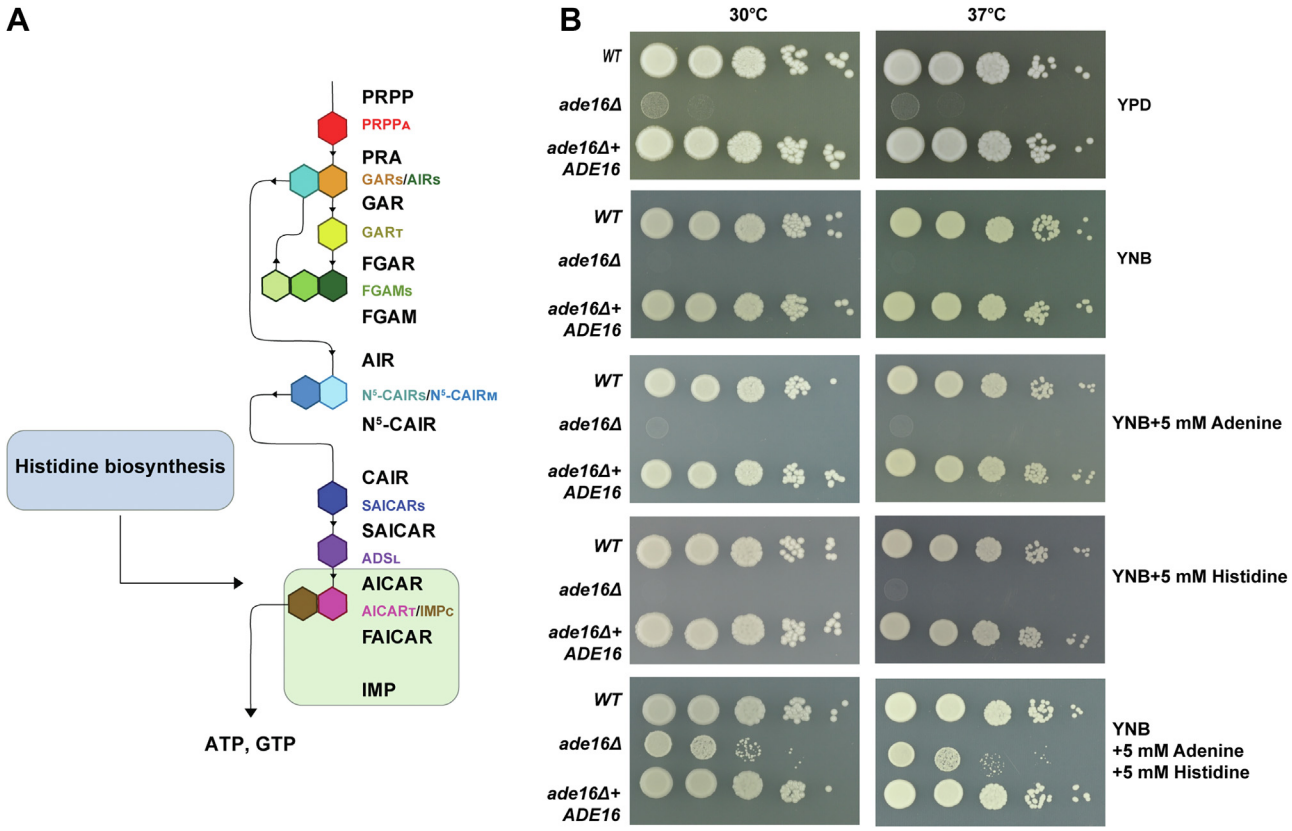

Figure 1. *Cryptococcus neoformans ade16Δ* mutants are adenine auxotrophs. *A*, *de novo* purine biosynthesis pathway. The bifunctional AICAR transformylase/IMP cyclohydrolase encoded by *ADE16* in *Cryptococcus neoformans* catalyzes the last two steps in the creation of IMP. Purine biosynthesis enzymes are represented as colored hexagons. Enzyme fusions are represented by hexagons joined together. *B*, Loss of *ADE16* results in adenine and histidine auxotrophy. Growth of 10-fold serial dilutions of WT, *ade16Δ*, and *ADE16* + *ade16Δ* strains of *C. neoformans* on a variety of media. Pictures were taken after 48 h of growth. The *ade16Δ* strain shows no growth on YNB agar without supplementation with adenine and histidine. AICAR, 5-aminoimidazole-4-carboxamide ribonucleotide; IMP, 5′-inosine monophosphate; YNB, yeast nitrogen base.

archaeal species, however, an unrelated protein performs the same activity, and it is this phylogenetically unrelated protein that is most common in bacteria and is the only form found in the eukaryotes. In contrast to the archaeal form, this more common AICAR transformylase employs N^{10}-formyl-tetrahydrofolate (N^{10}-fTHF) as the formyl group donor. In most archaea, the next step of the pathway, closure of the pyrimidine ring (completing formation of the purine base), occurs *via* elimination of water from FAICAR by the IMP cyclohydrolase PurO and cyclization to produce IMP. Once again, there is a more common and phylogenetically unrelated IMP cyclohydrolase, which is rare in the archaea, the most common form in bacteria, and is the only form found in eukaryotes to date; in this case, the biochemical reaction catalysis is identical between the two types of this enzyme. Beyond this phylogenetic distinction, there is an important structural distinction as well: species that have these more common forms of AICAR transformylase and IMP cyclohydrolase usually have them fused into a single protein dubbed ATIC (AICAR transformylase/IMP cyclohydrolase). This is the case in fungi and humans (19).

Each ATIC monomer comprises two distinct domains. The C-terminal domain is responsible for the AICAR transformylase activity. The N-terminal domain is responsible for the IMP cyclohydrolase activity (20). The fusion enzyme has been characterized with the aid of multiple crystal structures derived from avian, bacterial, and human sources (13, 15, 21), revealing an extensively intertwined homodimeric structure in which the transformylase and cyclohydrolase active sites are ∼50 Å apart, linked by a β-ribbon essential for dimerization (22, 23).

The only fungal species in which ATIC has been genetically characterized is *Saccharomyces cerevisiae*, where it is encoded by the ohnologs *ADE16* and *ADE17*. *S. cerevisiae ade16Δ ade17Δ* double mutants were found to be adenine and histidine auxotrophs (24). The adenine auxotrophy arises because of the defect in purine biosynthesis. Histidine auxotrophy arises because histidine and purine biosynthesis are interlinked; the histidine biosynthesis pathway enzyme imidazole glycerol phosphate synthase converts phosphoribulosyl-formimino-AICAR into imidazole glycerol phosphate (used to create histidine) and AICAR (which feeds into purine biosynthesis). Loss of ATIC results in an accumulation of AICAR and a negative feedback loop that inhibits ATP phosphoribosyltransferase, the first enzyme of histidine biosynthesis, resulting in histidine auxotrophy (24–27). Importantly, AICAR production by the histidine pathway alone is insufficient for robust *de novo* purine biosynthesis, as

indicated by the adenine auxotrophy of mutants lacking purine biosynthesis enzymes for the steps prior to AICAR synthesis (28).

While the purine biosynthesis pathway has been identified as a source of antiproliferation therapies for the treatment of cancer, anthrax, and tuberculosis (29–31), the investigation of purine metabolism in antifungal development has been limited. In *C. neoformans*, a number of mutants have been generated that affect the final steps of the biosynthesis of either AMP or GMP. They lead to an abolishment of virulence, suggesting the pathway could be a good target for therapeutic intervention (28, 32–34). In the search of a good antifungal target, it may be beneficial to investigate earlier steps in the pathway, prior to the formation of IMP.

Here, we describe an investigation of ATIC encoded by *ADE16* in *C. neoformans*. Molecular genetic analyses revealed that as with other purine biosynthesis mutants, the *ade16Δ* mutant is unable to successfully infect mice in an inhalation model of virulence. Characterization of the AICAR transformylase and IMP cyclohydrolase activities of this bifunctional protein and determination of its crystal structure have provided insight into key differences between the human and *C. neoformans* enzymes. Taken together, these findings create a platform for exploring *C. neoformans* ATIC as the target for antifungal drug development.

Results

Identification of the gene encoding AICAR transformylase and IMP cyclohydrolase in C. neoformans

S. cerevisiae has two ATIC-encoding genes, *ADE16* and *ADE17*, with products that share 85% amino acid sequence identity. To identify the equivalent gene(s) in *C. neoformans*, we employed the *S. cerevisiae* Ade16 and Ade17 proteins in reciprocal best-hit BLAST analyses. *CNAG_00700* was the only locus identified, consistent with *C. neoformans* having the bifunctional form of the enzyme found in all other eukaryotes to date, and it being encoded by a single gene. A protein alignment of *S. cerevisiae* Ade16 and Ade17 with *C. neoformans* Ade16 revealed 61.8 and 65.1% identity, respectively. As with other *C. neoformans* genes, we named *CNAG_00700 ADE16* based on the *S. cerevisiae* nomenclature. Comparison of the *C. neoformans* bifunctional Ade16 protein alignment with the equivalent *Homo sapiens* AICAR transformylase and IMP cyclohydrolase enzyme domains revealed an identity of 61.2%.

ADE16 *is essential for adenine and histidine prototrophy in* C. neoformans

To determine whether ATIC was required for virulence of *C. neoformans*, we performed a targeted deletion of the *C. neoformans ADE16* gene *via* biolistic transformation of the type strain H99O. The *ade16Δ* mutant obtained was subsequently complemented by introducing a WT copy of the gene into Safe Haven 1 (35) to create the *ade16Δ* + *ADE16* strain. Like the equivalent mutants in other species, the *C. neoformans ade16Δ* mutant could not grow on yeast nitrogen base (YNB) minimal media but could grow, albeit with a slight impairment, on YNB media supplemented with both histidine and adenine (Fig. 1*B*). The mutant was not able to grow on YNB supplemented with either adenine or histidine alone, as has been shown in *S. cerevisiae* (24). The complemented strain showed a restoration of the WT phenotype. Unusually, the *ade16Δ* mutant was not able to utilize the adenine and histidine present in rich yeast extract–peptone–dextrose (YPD) media; the reason for this phenotype is unknown (Fig. 1*B*).

Loss of Ade16 affects C. neoformans *virulence traits*

After confirming Ade16 is component for *de novo* biosynthesis, we next investigated whether deletion of the gene influences key virulence-associated traits. *C. neoformans* produces melanin to protect itself from oxidants produced by host cells (36), employs proteases to disseminate into the lungs and the central nervous system (37), and has a polysaccharide capsule that protects it against the immune system during infection (38).

To investigate any possible effects of the loss of ATIC on these virulence traits, the *ade16Δ* and *ade16Δ* + *ADE16* strains were tested in a range of *in vitro* phenotypic assays; to obviate the dual auxotrophies of the mutant, all media were supplemented with both adenine and histidine. There was no noticeable difference in the production of melanin with *ade16Δ* mutant compared with the WT or complemented strains (Fig. S1*A*). However, production of proteases was reduced in the *ade16Δ* mutant at both 30 and 37 °C (Fig. S1*B*), and the *ade16Δ* strain also displayed reduced capsule size at both temperatures (Fig. S1*C*). Combined with the dual auxotrophies, this provided evidence that the *ade16Δ* mutant was highly likely to exhibit impaired virulence.

ADE16 *is crucial for virulence in a murine inhalation model*

To confirm ATIC as a potential antifungal target, we investigated the effect of the *ade16Δ* mutation on virulence using a murine inhalation model of cryptococcosis. Ten mice per strain were infected with the WT, *ade16Δ*, and *ade16Δ* + *ADE16* strains. Infected mice were monitored daily and sacrificed when they lost 20% of body weight or showed symptoms of disease; the mice infected with the WT and complemented strains were euthanized after approximately 3 weeks. In contrast, all *ade16Δ* mutant–infected mice showed no outward signs of infection and were eventually culled 50 days post-inoculation (Fig. 2*A*). Organ burden assays of the mice infected with the *ade16Δ* mutant showed no *C. neoformans* colonies, indicating that in the absence of *ADE16*, *C. neoformans* is incapable of causing an invasive infection or even surviving in a latent form within this model host (Fig. 2*B*).

Expression, purification, and characterization of the oligomeric state of ATIC

To purify *C. neoformans* ATIC for enzymatic and structural characterization, *ADE16* was expressed in *Escherichia coli* and purified *via* immobilized metal affinity chromatography and

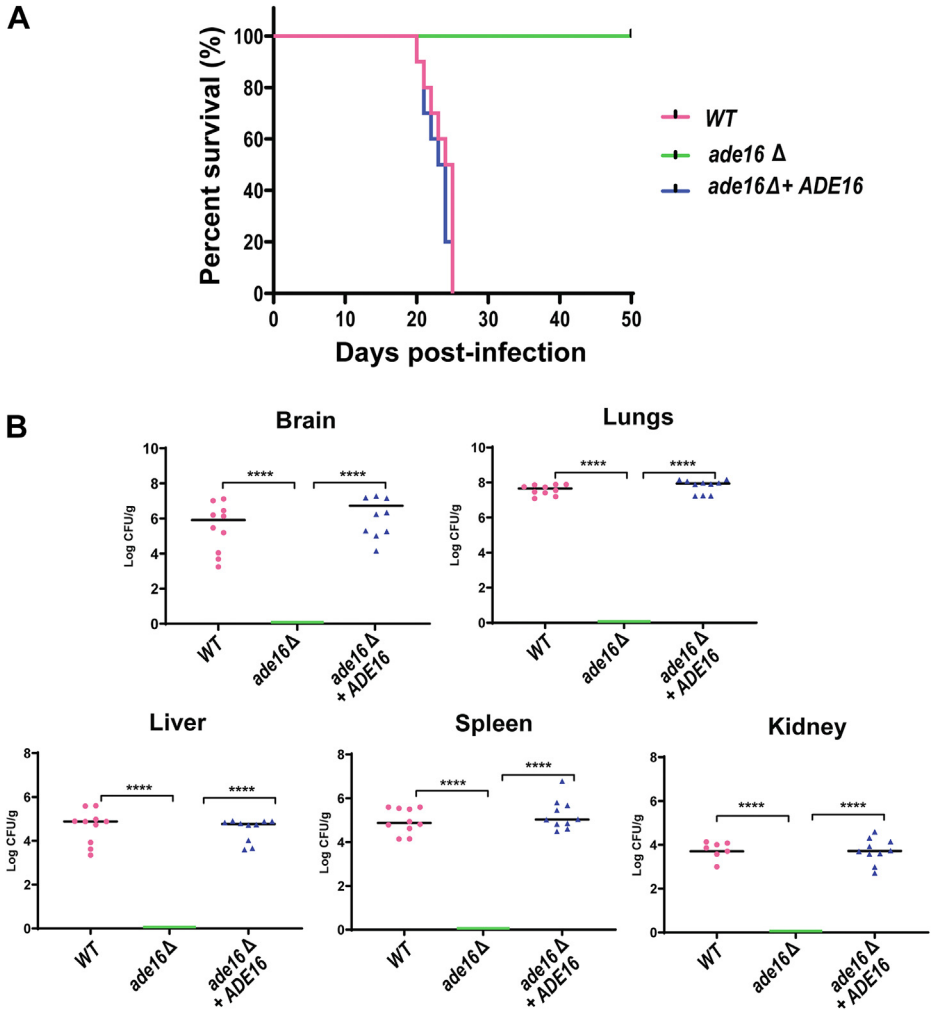

Figure 2. *ADE16* is essential for *Cryptococcus neoformans* virulence in a murine inhalation infection model. *A*, virulence of *ade16*Δ in a murine model of infection. BALB/c female mice were infected with 5×10^5 cells of the WT, *ade16Δ*, or *ADE16* + *ade16Δ* strains *via* nasal inhalation. Survival of mice was checked twice daily for 50 days. Kaplan–Meier survival curves were plotted, and significance was determined by log-rank tests. Mice infected with the *ade16Δ* mutant survived, whereas there was no significant difference between the survival of mice infected with the WT and *ade16Δ* + *ADE16* complemented strains ($p > 0.0001$). *B*, fungal organ burden of mice infected with WT, *ade16*Δ mutant, and *ade16Δ* + *ADE16* complemented strains. Organs collected from the mice after euthanasia were homogenized and spotted on YNB plates supplemented with adenine and histidine. The fungal burden for mice infected with the WT and *ade16* + *ADE16* was significantly higher (****$p < 0.0001$) than the mice infected with the *ade16Δ* mutant, which did not have any fungus present. Posthumous organ burden was calculated in colony-forming units (CFUs) per gram of brain, lungs, kidney, spleen, and liver. YNB, yeast nitrogen base.

size-exclusion chromatography (SEC), yielding a single band of molecular mass ~65 kDa on SDS-PAGE (Fig. S2*A*). In order to characterize the oligomeric state of ATIC, we used multiangle laser light scattering (MALS) coupled to SEC. SEC–MALS indicated that the molecular weight of ATIC was approximately 140 kDa in solution. This indicates that the *C. neoformans* AICAR transformylase/IMP cyclohydrolase forms a homodimer *in vitro*, which is in agreement with the oligomeric states reported for the human, avian, and *E. coli* enzymes (13, 15, 21) (Fig. S2*B*). Mass photometry analyses supported this observation, with Ade16 showing a molecular weight of approximately 140 kDa with this technique as well (Fig. S2*C*).

Determination of the enzyme kinetic properties of C. neoformans *ATIC*

Given that ATIC is vital to *C. neoformans* for successful infection in a murine inhalation model, we extended our investigation to study the biochemical function of this enzyme and identify possible functional differences between the human and fungal enzymes that could be exploited in drug development. Pure recombinant ATIC was used to study the steady-state parameters of the enzyme; activity assays were optimized as part of the study and then performed at the optimal conditions at pH 7.5 and 37 °C.

AICAR transformylase activity

ATIC catalyzes the final two steps of the formation of the first purine, IMP. In the penultimate step, the AICAR transformylase domain catalyzes the transfer of a formyl group from N^{10}-fTHF to the 5-amino group of AICAR to yield FAICAR and THF (Fig. 3*A*). This activity was assayed *in vitro* by varying the concentration of AICAR and measuring the formation of THF through the corresponding increase in absorbance at 298 nm. The AICAR transformylase activity followed

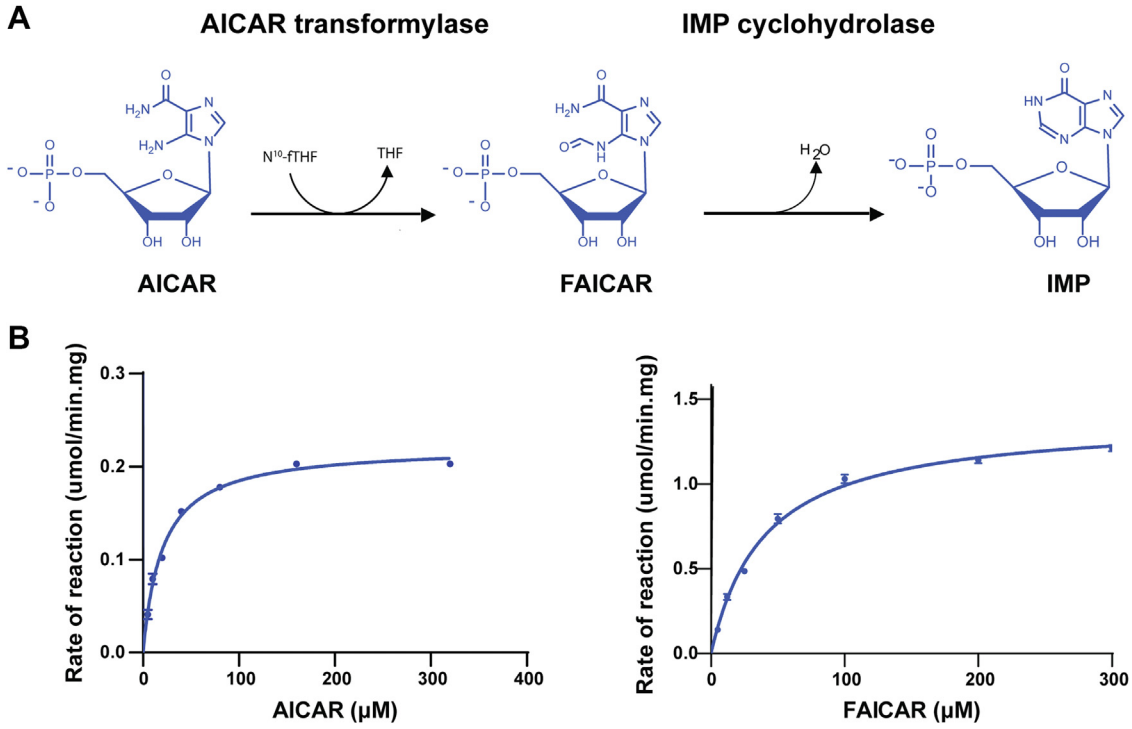

Figure 3. Enzyme kinetics of *Cryptococcus neoformans* ATIC. *A*, the two chemical reactions carried out by ATIC; first, the formyl group is added to AICAR to create formyl AICAR (FAICAR). Second, the purine ring is completed to form IMP. *B*, activity of *C. neoformans* ATIC with different concentrations of AICAR (AICAR transformylase activity) or FAICAR (IMP cyclohydrolase activity). Data were collected as described in the Experimental procedures section, and each data point represents the average of three independent determinations. Curve and data points (mean with standard error) were fit to the Michaelis–Menten equation using direct nonlinear fitting. AICAR, 5-aminoimidazole-4-carboxamide ribonucleotide; ATIC, AICAR transformylase/5′-inosine monophosphate cyclohydrolase; IMP, 5′-inosine monophosphate.

Michaelis–Menten kinetics with K_{m_app} of 130 ± 10 μM, V_{max} of 6.7 ± 0.1 U/mg, and k_{cat} of 7.5 ± 0.1 s^{-1} for AICAR as the substrate (Fig. 3*B*).

Enzymatic parameters for AICAR transformylase have been reported for one bacterial species (*Staphylococcus lugdunensis*), one fungal species (*S. cerevisiae*), and two metazoan species (*Gallus gallus* and *H. sapiens*) (23, 24, 39–41) (Table 1). Compared with previously characterized AICAR transformylases, the kinetic parameters of the *C. neoformans* enzyme were different from the *S. cerevisiae* and metazoan enzymes. The *C. neoformans* ATIC $K_{m\_app\ AICAR}$ (130 ± 10 μM) was eight times higher than *S. cerevisiae* Ade16 (26 μM) and Ade17 (22 μM). Comparisons with the metazoan species indicated that the *C. neoformans* ATIC $K_{m\_app\ AICAR}$ (130 ± 10 μM) is also approximately eight times higher than the reported $K_{m\_app\ AICAR}$ for the human enzyme (16.8 ± 1.5 μM) and *G. gallus* enzyme (15.2 ± 3.6 μM) and four times higher than the values reported for the bacterial enzyme (32 ± 2.5 μM). AICAR turnover (k_{cat}) (7.5 ± 0.1 s^{-1}) of the *C. neoformans* enzyme was nearly 2.5 times greater than human enzyme (2.9 ± 0.1 s^{-1}).

IMP cyclohydrolase activity

The IMP cyclohydrolase domain of ATIC performs the final ring closure reaction, converting FAICAR to IMP, with the elimination of a water molecule (Fig. 3*A*). The IMP cyclohydrolase assay was performed *in vitro* by varying the concentration of FAICAR and measuring the production of IMP through the corresponding increase in absorbance at 248 nm. The IMP cyclohydrolase activity followed Michaelis–Menten kinetics, with a $K_{m\_app\ FAICAR}$ value of 30 ± 1 μM, V_{max} of 8.6 ± 0.1 U/mg, and k_{cat} of 7.7 ± 0.1 s^{-1} for FAICAR as the substrate (Fig. 3*B*).

Again, the *C. neoformans* IMP cyclohydrolase $K_{m\_app\ FAICAR}$ (30 ± 1 μM) was higher (20 and 14 times) than those reported for the human (1.4 ± 0.1 μM) and bacterial enzymes (2.1 ± 0.3 μM), whereas the turnover number (k_{cat}) of IMP cyclohydrolase was similar to the human protein. In addition, when compared with the available data for other species, the *C. neoformans* protein had the highest specific activity for both reactions.

Overall, these results not only prove that the identified *C. neoformans* gene encodes a bifunctional enzyme catalyzing both the AICAR transformylase and IMP cyclohydrolase activities but also show that there are functional differences between the fungal and metazoan enzymes, with variations in the observed values for specific activity, k_{cat} and K_{m_app}. These functional differences could potentially be exploited in the rational design of fungus-specific inhibitors.

Crystal structure of C. neoformans *ATIC*

The long-term goal of our work is the design of potential antifungal drugs that bind selectively to fungal ATIC. It is therefore beneficial to understand the structure of the

Table 1
Comparison of reported kinetic parameters of ATIC from multiple species

Species	V_{max} (AICAR) (U/mg)	k_{cat_app} (AICAR) (s^{-1})	K_{m_app} (AICAR) (μM)	V_{max} (FAICAR) (U/mg)	k_{cat_app} (FAICAR) (s^{-1})	K_{m_app} (FAICAR) (μM)	Reference
Cryptococcus neoformans	6.7 ± 0.1	7.5 ± 0.1	130 ± 10	8.6 ± 0.1	7.7 ± 0.1	30 ± 1	This work
Saccharomyces cerevisiae							
Ade16	1.0 ± 0.1	ND	26	1.7 ± 0.4	ND	ND	(23)
Ade17	0.9 ± 0.1		22	2.0 ± 0.5			
Homo sapiens	1.7 ± 0.6	2.9 ± 0.4	16.8 ± 1.5	2.8 ± 0.01	6.0 ± 0.8	1.4 ± 0.1	(22)
Gallus gallus	2.7 ± 0.2	ND	15.2 ± 3.6	ND	ND	ND	(39)
Staphylococcus lugdunensis	0.5 ± 0.0	ND	32.4 ± 2.5	2.6 ± 0.5	ND	2.1 ± 0.3	(37)

Abbreviation: ND, no data.
Kinetic parameters for AICAR transformylase and IMP cyclohydrolase activities of *C. neoformans* ATIC, compared with published values from other species. Values are shown ± standard error.

C. neoformans protein to enable exploitation of the differences to the human enzyme for the design of fungus-specific inhibitors. To enable comparisons between the *C. neoformans* enzyme and those from other species, and to identify targetable species-specific features, we used X-ray crystallography to determine the crystal structure of the *C. neoformans* ATIC at 2.67 Å resolution (Protein Data Bank [PDB] code: 7MGQ). The structure was determined by molecular replacement using the human ATIC structure (PDB code: 1PKX) as the search model (42). The asymmetric unit has four molecules (A, B, C, and D), corresponding to two ATIC homodimers. The overall structure is similar to the well-characterized *G. gallus* (PDB code: 1M9N) and *H. sapiens* enzymes (42, 43). The superposition of *C. neoformans* ATIC onto the ligand-bound AICAR avian and human ATIC yields an overall RMSD of 1.2 and 1.0 Å over 1210 Cα atoms (chain A and chain B), with sequence identity of 60% and 61%, respectively. The loop connecting the IMP cyclohydrolase and AICAR transformylase domains is 15 residues longer in *C. neoformans* ATIC than in avian and human ATIC (Fig. S3). This loop is located away from the AICAR transformylase and IMP cyclohydrolase active sites and is unlikely to play a role in catalysis but may contribute to the stability of the enzyme dimer. We hypothesize that this region could be targeted with compounds that can selectively bind in *C. neoformans* ATIC and that would inhibit the function of the enzyme.

Each monomer has an N-terminal IMP cyclohydrolase domain (residues 1–197) and a C-terminal AICAR transformylase domain (212–605), and the active sites of each were inferred based on sequence alignments and comparison with the ligand-bound structure of the avian and human ATIC enzymes (Fig. 4). AICAR and XMP were cocrystallized with

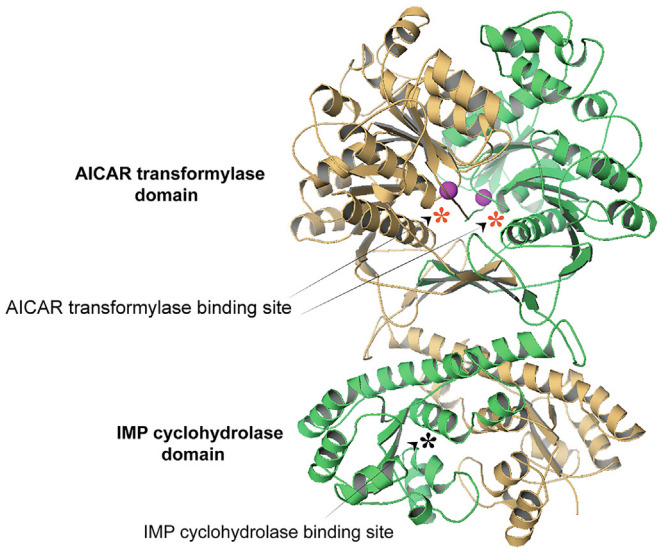

Figure 4. *Cryptococcus neoformans* ATIC crystal structure. Crystal structure of *C. neoformans* ATIC dimer. Monomer A is colored *brown*, and monomer B is colored *green*. The two *magenta spheres* represent bound magnesium ions. *Asterisks* in *black* and *orange* represent the approximate position of IMP cyclohydrolase and AICAR transformylase active sites, respectively. ATIC, AICAR transformylase/5′-inosine monophosphate cyclohydrolase; IMP, 5′-inosine monophosphate.

the avian ATIC and were found to bind to the AICAR transformylase and IMP cyclohydrolase active sites, respectively. XMP was cocrystallized with the human ATIC and found bound to only one of the two IMP cyclohydrolase active sites in the homodimer.

AICAR transformylase domain

Studies of the structure of the AICAR transformylase domain have been performed in *H. sapiens*, *G. gallus*, *Thermotoga maritima*, and *Mycobacterium tuberculosis* (13, 15, 43, 44). Like the avian and human proteins, the AICAR transformylase domain of *C. neoformans* ATIC is divided into three subdomains, with the two major subdomains, subdomain 1 and subdomain 3, each composed of a central six-stranded β-sheet surrounded by four α-helices, and these are separated by the smaller subdomain 2 (Fig. 5*A*). Electron density for residues 489 to 495 and 514 to 519 of chain B, and 513 to 516 of chain C in *C. neoformans*, ATIC was poorly defined, which is likely because of the structure flexibility in this region. The two AICAR transformylase active sites are at the interface between the two monomers, with residues from both lining the binding sites. When compared with the avian and human ATIC, the residues of the AICAR transformylase active site in *C. neoformans* ATIC are completely conserved, including the two key catalytic residues Lys267 and His268 (42). In this regard, the AICAR transformylase active site may not be very suitable for the design of species-specific inhibitors (Fig. 5*B*).

Even though *C. neoformans* ATIC has no ligand bound, a magnesium ion is found in subdomain 3 in each monomer, in the place of a potassium ion reported in the previous ATIC structures. In structures reported previously, a potassium ion was modeled in domain 3 and suggested to play a key role in stabilization of the tertiary structure (15, 42, 43). Here in the *C. neoformans* structure, the ion is most likely a magnesium ion, based on its hexacoordinate state and the crystallization solution. It makes interactions with the backbone carbonyl group of residues Leu436, Thr439, and Leu602, the side-chain hydroxyl group of residues Ser441 and Ser443, and the side-chain carboxyl oxygen of Asp552. The peptide bond between Ser441 and the adjacent residue Asn442 is in a *cis* conformation, which is consistent with all ATIC structures and responsible for the orientation of ligand-binding residues in the active site (Fig. S4) (15).

IMP cyclohydrolase domain

Like the AICAR transformylase domain, the structure of the IMP cyclohydrolase domain of ATIC has previously been determined for the enzymes from *H. sapiens*, *G. gallus*, *T. maritima*, and *M. tuberculosis* (13, 15, 43, 44). These four structures exhibit a Rossman fold topology, consisting of a parallel five-stranded β-sheet with strand order 3-2-1-4-5, surrounded by three α-helices on one side of the sheet and seven on the other side (in the *C. neoformans* structure, one of the β-strands does not fulfill the criteria used by PyMOL (Schrödinger, LLC) to assign it as this element of secondary structure; Fig. S5*A*).

Each of the two IMP cyclohydrolase active sites in the homodimer are formed with residues from a single monomer. This site undergoes major conformational changes after XMP binding in *H. sapiens* and *G. gallus* (Fig. 6, *A* and *B*) In human ATIC, XMP binding causes a side-chain flip of the conserved residues Tyr104 and Lys66 and inward movement of the loops 103 to 106 and 56 to 71 (numbers based on *C. neoformans* ATIC), which are located at the rim on the opposite sides of the active site. The movement of these loops converts the IMP cyclohydrolase active site to a closed conformation. The *C. neoformans* IMP cyclohydrolase active site has no ligand present and adopts an open conformation (Fig. 6, *A* and *B*).

We focused on the comparison of active-site residues in *C. neoformans* and human ATIC to identify nonconserved residues and structural differences in the enzymes that could be exploited for the design of species-specific ATIC inhibitors. The *C. neoformans* IMP cyclohydrolase active-site region contains residues Arg65, Lys67, Thr68, Tyr105, Asp126, Ile127, and Gly128, each of which are present in the human and avian IMP cyclohydrolase active sites (Fig. 5*B*). By contrast, Ser12 in human ATIC, a key residue that makes a hydrogen bond with the ribose ring of XMP and is conserved in animals and plants, is substituted with a tyrosine (Tyr13) in *C. neoformans*, *M. tuberculosis*, and other fungi (Fig. S3). Although both serine and tyrosine carry a hydroxyl group, which can form hydrogen bonds, tyrosine also contains an aromatic ring, which is bulkier than the short serine side chain.

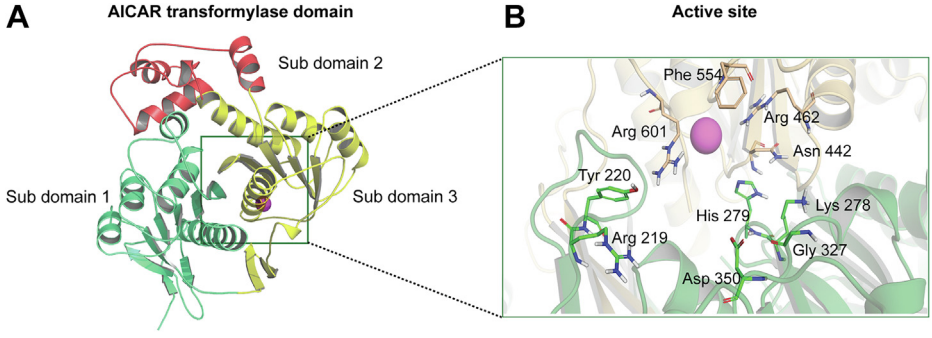

Figure 5. Crystal structure of *Cryptococcus neoformans* AICAR transformylase domain. *A*, structure of *Cryptococcus neoformans* AICAR transformylase domain of monomer A (residues 212–605), colored by subdomains 1 to 3. The magnesium ion is presented as a *magenta sphere*. *B*, close-up view of the active site of AICAR transformylase. The residues of the AICAR transformylase active site in *C. neoformans* ATIC are shown in *stick* representation. AICAR, 5-aminoimidazole-4-carboxamide ribonucleotide.

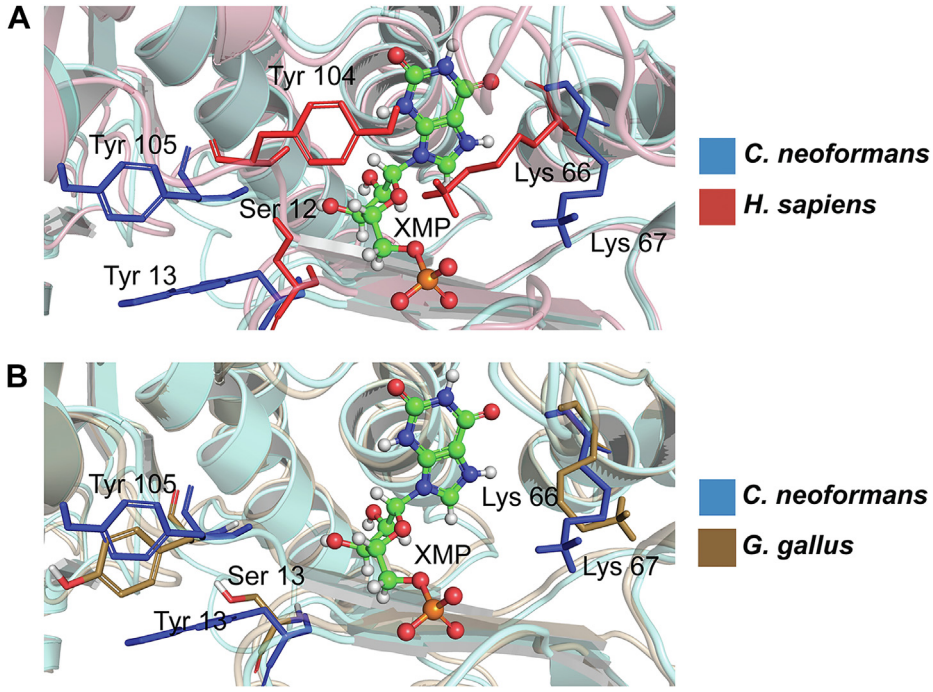

Figure 6. Comparison of the active sites of IMP cyclohydrolases from *Cryptococcus neoformans*, *Homo sapiens*, and *Gallus gallus*. Structural comparison of IMP cyclohydrolase active sites by superposition of *A, Homo sapiens* ATIC (*red*) closed form and *C. neoformans* ATIC (*blue*) open form. *B, G. gallus* ATIC (*brown*) open form and *C. neoformans* ATIC (*blue*) open form. The XMP bound in human ATIC has been superimposed. In the IMP cyclohydrolase, active-site tyrosine and lysine residues, located at the opposite sides, maintain the open and closed states upon XMP binding, which can be clearly observed in the comparison of *H. sapiens* ATIC and *C. neoformans* ATIC. Ser12 in *H. sapiens* ATIC is substituted with a tyrosine (Tyr13) in *C. neoformans* ATIC. ATIC, AICAR transformylase/5′-inosine monophosphate cyclohydrolase; IMP, 5′-inosine monophosphate.

This is a key difference that could potentially be exploited to design compounds for fungus-specific ATIC inhibition.

Discussion

C. neoformans poses a significant health threat to the immunocompromised population worldwide. The current range of antifungals is inadequate in the treatment of this fungal disease because of high toxicity, increasing prevalence of resistant strains, and drug crossreactivity. Therefore, it is of rising importance to identify new drug targets to meet this need; new therapy for *C. neoformans* could have a significant effect on the morbidity and mortality in immunocompromised patients. Our characterization of the bifunctional enzyme AICAR transformylase/IMP cyclohydrolase that performs the last two steps in the purine biosynthetic pathway has shown its potential as a target for the treatment of fungal infections.

Our investigation of the ATIC-encoding *ADE16* gene and its dual enzymatic functions in *C. neoformans* make this the first species in which ATIC loss-of-function mutants, enzymatic activity, and structure have all been characterized. We have demonstrated that the *ade16Δ* mutant, like its *S. cerevisiae* double mutant counterpart, is an adenine and histidine auxotroph. However, even with supplementation, *in vitro* assays clearly demonstrate that the growth of *ade16Δ* mutants is still impaired compared with WT *C. neoformans*. In addition, *ade16*Δ mutants are also unable to scavenge adenine or histidine from nutrient-rich YPD media, similar to other mutants in the *de novo* purine pathway in *C. neoformans* (32).

To determine whether this defect influences the ability to cause infection, the *ade16*Δ mutant was employed in a murine inhalation model of infection. The mutant was unable to cause symptoms of meningoencephalitis, consistent with organ burden data revealing that the *ade16*Δ mutant strain was cleared. This result reconfirms that *C. neoformans* is highly dependent on *de novo* purine biosynthesis during infection of the purine-poor central nervous system (45). Together, the *in vitro* phenotypic assays and the *in vivo* virulence model show that ATIC could be a very useful drug target.

To determine the suitability of this enzyme as a drug target, we investigated its biochemical activity and structure and compared them with the ortholog from the human host. Differences in the kinetic parameters identified between orthologous enzymes may indicate that the substrates interact differently with the active site, highlighting that it may be possible to design inhibitors that specifically exploit the unique properties of the ATIC *C. neoformans* enzyme. However, the findings showing that *C. neoformans* ATIC protein had lower affinity for substrates compared with the human protein could present difficulties in identifying an inhibitor that specifically targets the fungal enzyme. An inhibitor such as a substrate analog is unlikely to be suitable, as the analog might inhibit the human enzyme more strongly than to the fungal enzyme. Thus, the structure determined for *C. neoformans* ATIC is crucial for the design of a potential fungal enzyme inhibitor specifically targeting features found in the fungal enzyme.

While determination of the crystal structure of *C. neoformans* ATIC revealed that the human and fungal structures have a high level of conservation, unique elements were identified in the fungal enzyme. In the active-site pocket of the IMP cyclohydrolase domain, the serine residue in the human enzyme is replaced with a tyrosine residue in *C. neoformans* and other fungi, leading to surface changes in the active-site pocket that may be exploited for the design of fungal enzyme–specific ligands. Comparison of the *C. neoformans*, human, and avian ATIC structures also shows that the loop that connect the IMP cyclohydrolase domain and the AICAR transformylase domain is longer (15 residues) in *C. neoformans.* These structural differences could be utilized during the process of inhibitor design, aiming to specifically target these differentiating features, the amino acid differences, and the longer loop between domains, found in the fungal enzyme.

As enzyme interfaces are usually less conserved compared with the highly conserved active sites, it may be even more effective to design drugs that target protein interfaces (46). A recent study revealed that a small compound inhibitor Cpd14 inhibited AICAR transformylase *via* disruption of ATIC homodimerization (47). The longer loop found between the domains could be a potential site to target for inhibitor design for prevention of homodimer formation essential for ATIC function.

Development of a novel antifungal compound benefits significantly from having a crystal structure available, to identify exploitable differences between the target species, in this case *C. neoformans*, and the human host. The structure of *C. neoformans* ATIC revealed differences in active-site accessibility and potential binding orientation, compared with the human enzyme, which could be exploited during antifungal drug design to create an inhibitor specific to *C. neoformans* or fungi in general. Beyond addressing this important infectious disease–related need, our comprehensive molecular genetics, virulence, and kinetic and structural analyses make the *C. neoformans* enzyme a strong model with which to further investigate the function of ATIC across the domains of life.

Experimental procedures

Bioinformatics analyses

ADE16 gene sequences of the *C. neoformans* type strain H99O used in this study were obtained from the published genome sequence (48). The gene encoding ATIC was identified *via* reciprocal hit BLAST analysis queried with the *S. cerevisiae* Ade16 and Ade17 sequences. Sequence alignments of ATIC from *C. neoformans*, *S. cerevisiae*, *H. sapiens*, *Gallus gallus*, and *M. tuberculosis* were performed by ESPript (49).

Media and strains

All strains are listed in Table S1. H99O and *ade16*Δ + *ADE16* complementation strains were grown on nutrient-rich YPD (2% bactopeptone, 1% yeast extract, 2% glucose) media solidified using 2% agar. All strains were cultured at 30 °C. The *ade16*Δ strains were grown on 0.45% YNB, 1% ammonium sulfate, and 2% glucose supplemented with 5 mM histidine and 5 mM adenine. *E. coli* was grown on lysogeny broth (1% tryptone, 0.5% yeast extract, and 1% sodium chloride) media supplemented with 100 μg/ml ampicillin for the selection of colonies and cultured at 37 °C. *E. coli* was grown in auto-induction media (0.5% yeast extract, 1% tryptone, 2% and 0.5% glycerol, 0.05% glucose, 0.2% lactose, 0.5 M $(NH_4)_2SO_4$, 0.5 M KH_2PO_4, 1 M Na_2HPO_4, and 1 mM $MgSO_4$) for large-scale protein expression.

Creating ADE16 *gene deletion and complementation strains*

All primers (IDT) used in this study are listed in Table S2 and plasmids in Table S3. Phusion High Fidelity polymerase (New England Biolabs) was used for generation of all PCR amplicons.

PCR fragment of 1 kb upstream of *ADE16* (UQ4336, UQ3294), the G418 resistance marker (UQ3295, UQ3296), and 1 kb downstream of *ADE16* (UQ3297, UQ4337) were combined *via* overlap PCR (UQ4336, UQ4337) to create a deletion construct that was cloned into EcoRI and BamHI cut-pBlueScriptII SK(−) using NEBuilder HiFi DNA Assembly (New England Biolabs) to give pMSIW8. H99O and pJAF1 were used as a template to amplify *ADE16* and amplify G418 resistance marker, respectively (50).

Following digestion with NdeI and SpeI, biolistic transformation of the deletion construct was performed using a Bio-Rad He-1000 Biolistic device into the type strain H99O strain on YNB media supplemented with 1 mM adenine, 1 mM histidine, 1 M sorbitol, and 5 μg/ml W7 hydrochloride (51, 52). *C. neoformans* cells recovered overnight were then scraped onto YNB media supplemented with 1 mM adenine, 1 mM histidine, and G418 to select for G418-resistant colonies. Colonies that subsequently formed on selective plates were tested for adenine auxotrophy on YNB media without adenine supplementation. To confirm that the *ADE16* gene was deleted, Southern blotting was performed using the *ADE16* region (UQ4336 and UQ4337) as a probe.

Complementation of the *ade16*Δ mutant was performed by the reintroduction of *ADE16* at the Safe Haven Locus in chromosome 1 (35). The *ADE16* region, including 1 kb upstream, the ORF, and 1 kb downstream, was amplified from the *C. neoformans* type strain H99O genomic DNA (primers UQ4336 and UQ4337). The product was digested sequentially with XbaI and SacI and then cloned into ClaI and HindIII-cut Safe Haven targeting vector pSDMA25 using NEBuilder HiFi DNA Assembly to create pMSIW8. Sanger sequencing was used to verify the sequence was error free. The plasmid pMSIW7 was linearized with PacI and biolistically transformed into the *ade16*Δ mutant on YNB media supplemented with 1 M sorbitol, 1 mM adenine, 1 mM histidine, and 5 μg/ml W7 hydrochloride. The overnight recovered transformants were selected on YPD media supplemented with 100 μg/ml nourseothricin. Transformant colonies were screened by diagnostic PCR (UQ1768, UQ2962, UQ2963, and UQ3348) and for adenine prototrophy (35).

Precise integration of *ADE16* at the Safe Haven location was verified by Southern blot by probing with the *ADE16* fragment (UQ4336 and UQ4337).

Phenotype and virulence assays

Mutant and complementation strain *in vitro* phenotypes were tested using serial dilution spotting assays; cells were suspended in 1 ml of distilled water to reach an absorbance of 1.0 at 600 nm, spotted on YPD, YNB, and YNB supplemented with 5 mM adenine, and 5 mM histidine, for the adenine and histidine auxotrophy, respectively, and incubated at 30 and 37 °C. For melanin and protease production, cells were spotted on L-3,4-dihydroxyphenylalanine agar supplemented with 1 mM asparagine and YNB agar supplemented with 1% bovine serum albumin (Sigma–Aldrich), respectively. All media were supplemented with 5 mM adenine and 5 mM histidine, and plates were incubated at both 30 and 37 °C.

For capsule production, strains were grown in RPMI1640 (Life Technologies) supplemented with 2% glucose, 10% fetal bovine serum (Life Technologies), 5 mM adenine, and 5 mM histidine in a shaking incubator at 30 and 37 °C for 24 h. Cells were stained with India ink (BD Diagnostics), viewed, and imaged using a Leica DM2500 microscope and DFC425C camera (Leica). Five images were photographed for each strain. The whole cell and cell body diameter of five cells from each image were measured using the ruler tool in Adobe Photoshop CC (Adobe Systems), and capsule measurement was presented as a relative percentage of cell size. The capsule assays were performed in triplicate. A one-way ANOVA test with Sidak's post test was used to determine significance of differences in capsule sizes between strains.

Mouse virulence experiments

Ten 6-week-old mice were intranasally infected with 5×10^5 cells of *C. neoformans* H99O WT strain, the *ade16*Δ mutant, and *ade16Δ + ADE16* complemented strain. Five mice were housed in an individually ventilated cage, which was lined with Bed-o'Cobs 1/8" bedding (The Andersons), Crink-L'Nest nesting material (The Andersons), and cardboard. Mice were provided with constant supply of Rat and Mouse Cubes (Specialty Feeds) and drinking water. After infection, the mice were monitored for signs of *C. neoformans* infection, scored, and weighed daily. When the mice lost 20% of their starting body weight or showed severe symptoms, they were euthanized by carbon dioxide inhalation. The spleen, liver, kidney, lungs, and brains were collected and homogenized using a TissueLyser II (QIAGEN). The organ suspensions were serially diluted and spotted on YPD agar supplemented with 100 μg/ml ampicillin, 50 μg/ml kanamycin, and 25 μg/ml chloramphenicol to prevent bacterial contamination. After 48 h, the colonies were counted to calculate the organ burden. The survival curves and organ burden plots were plotted using GraphPad Prism 7.0 (GraphPad Software, Inc). The log rank test and a one-way ANOVA with Tukey's multiple comparisons test were used to determine the significance of survival and the organ burden, respectively.

Ethics statement

This study was carried out in strict accordance with the recommendations in the Australian Code of Practice for the Care and Use of Animals for Scientific Purposes by the National Health and Medical Research Council. The protocol was approved by the Molecular Biosciences Animal Ethics Committee of The University of Queensland (AEC approval number: SCMB/010/17). Infection was performed under methoxyflurane anesthesia, and all efforts were made to minimize suffering through adherence to the Guidelines to Promote the Wellbeing of Animals Used for Scientific Purposes as put forward by the National Health and Medical Research Council.

Expression and purification of ATIC

Total RNA was isolated from YNB-grown strain H99O using TRIzol Reagent (Invitrogen), with intron-free complementary DNA and then synthesized using a Bioline complementary DNA synthesis kit (Bioline). The ATIC ORF was subsequently PCR amplified (primers UQ3615 and UQ3616), the product inserted *via* ligation-independent cloning into the SspI site of His-tag vector pMCSG7 (53), and transformed into competent *E. coli* BL21(DE3) pLysS cells for protein expression.

Cells were grown with shaking at 200 rpm at 37 °C until an absorbance reached 0.8 at 600 nm and then the temperature was dropped to 20 °C and incubated for an additional 20 h with shaking. Cells were harvested and resuspended in lysis buffer (3 ml/1 g; 50 mM Hepes [pH 8.0], 300 mM NaCl, 30 mM imidazole, 1 mM DTT, and 1 mM PMSF), before disruption with a Sonifier W450 Digital Ultrasonic Cell Disruptor sonicator (Branson). Following centrifugation to remove unbroken cells and cell debris, the supernatant was loaded onto a 5 ml HisTrap Fast Flow column (GE Healthcare), equilibrated with wash buffer, to purify the His-tagged protein by immobilized nickel-affinity chromatography. The protein was eluted in a linear gradient of 30 to 500 mM imidazole, showing a single elution peak. Peak fractions were pooled, concentrated, and further purified using a Superdex 200 SEC column (GE Healthcare) equilibrated in 10 mM Hepes (pH 7.5), 150 mM NaCl, and 1 mM DTT. All protein chromatography steps used an ÄKTApurifier FPLC system. Peak fractions were checked on SDS-PAGE and then combined and concentrated to ∼27 mg/ml and flash frozen in liquid nitrogen for storage at −80 °C.

Enzyme assays and kinetic analysis

All enzyme assays were performed using a Cary60 UV spectrophotometer (Agilent). Assays were performed in triplicate at 37 °C with purified enzyme. The AICAR transformylase activity assay used the method of Mueller and Benkovic (40). Reaction mixtures (1 ml) contained 33 mM Tris–Cl (pH 7.5), 25 mM KCl, 5 mM β-mercaptoethanol,

0.1 mM N^{10}-fTHF, and 0.05 mM AICAR. The reaction was started by addition of 10 μl *C neoformans* ATIC (2 mg/ml). AICAR transformylase activity was monitored by the absorbance increase at absorbance at 298 nm following the formation of FH_4 (54). To synthesize N^{10}-fTHF for the assay, 5,10-methenyltetrahydrofolate was initially synthesized following the procedure of Rabinowitz *et al.* (55). The precipitate was washed with cold ethanol, dried *in vacuo*, and stored at −20 °C. This intermediate was then used to create N^{10}-fTHF, as described Rayl *et al.* (23).

For the IMP cyclohydrolase assays, the method of Mueller and Benkovic was used (40). The reaction contained 100 mM Tris–Cl (pH 7.5) and 0.1 mM FAICAR in a total reaction volume of 1 ml. Purified *C. neoformans* ATIC (20 μg/ml) was added to start the reaction, and IMP cyclohydrolase activity monitored by the absorbance increase at an absorbance at 248 nm, corresponding to the production of IMP (40). FAICAR was synthesized following the protocol by Lukens *et al.* (56), and the product was analyzed by HPLC–MS.

The standard AICAR transformylase and IMP cyclohydrolase assays were used for determining the steady-state kinetic parameters for the *C. neoformans* enzyme. In the AICAR transformylase assay, the experiments were performed by varying the concentrations of AICAR (from 0.03 to 3.8 mM). In the IMP cyclohydrolase assay, the experiments were performed by varying the concentrations of FAICAR (from 0.005 to 0.3 mM). The reaction rate was plotted against the concentration of substrate. Data were fitted to the Michaelis–Menten equation using nonlinear regression to determine of substrate using GraphPad Prism, version 8.0.

MALS with SEC

SEC MALS was performed using a Dawn Heleos II 18-angle light-scattering detector coupled with an Optilab rEX refractive index detector (Wyatt Technology) and an inline Superdex 200 10/300 size-exclusion column (GE Healthcare). Experiments were done at an ATIC concentration of 5 mg/ml in SEC buffer (10 mM Hepes, pH 7.5, 150 mM NaCl, and 1 mM DTT) at room temperature, with a flow rate of 0.5 ml/min.

MP

A Refeyn OneMP instrument (Refeyn Ltd) was used to measure the oligomeric states of the proteins in solution. About 10 μl of gel filtration buffer followed by 1 μl of the protein solution was applied to the drop to a final concentration of 100 nM, and 6000 frames were recorded. The calibration curve was obtained by using three protein standards (66, 146, and 480 kDa) (Thermo Fisher Scientific).

Protein crystallization and crystal structure determination

Initial crystallization screens were performed using several commercial screens. All crystallization conditions were set up as hanging drop vapor diffusion at 20 °C using protein concentration of 12 mg/ml. Based on the initial crystal hits in the PACT screen, optimization yielded diffraction quality crystals in a solution containing 0.2 M $MgCl_2$, 20% w/v PEG 6000, and 0.2 M Tris base at pH 8. Before data collection, the crystals were soaked in 25% (v/v) glycerol for cryoprotection and then flash cooled in liquid nitrogen. Diffraction data (2.67 Å resolution) were collected at cryogenic temperatures from a single crystal at the Australian Synchrotron MX 1 beamline (57) at an X-ray wavelength of 0.954 Å. The data were then processed using XDS (58) and Aimless in the CCP4 Suite (59). The *C. neoformans* ATIC structure was solved by molecular replacement using Phaser in the PHENIX suite (https://phenix-online.org/) (60), with the human ATIC structure (PDB code: 1PKX) as the search model (42). The structure model was subsequently built using PHENIX AutoBuild (61) and refined using PHENIX. In between rounds of refinement, model building was conducted manually using Coot, version 0.8.9.2 (https://www2.mrc-lmb.cam.ac.uk/personal/pemsley/coot/) (62). Metal ions were modeled based on their peaks in the mF_O–DF_C difference density map, together by consideration of the *B*-factors with their coordination ligands, and chemical plausibility. The crystallization condition contained 0.2 M $MgCl_2$, which may be the reason for the presence of magnesium ion bound in the place of potassium ion that was found in the previous reported ATIC structures. Structure analyses were performed in PyMOL. The final R_{free} and R_{work} values were 0.23 and 0.20, respectively. The X-ray crystallography statistics for data collection and refinement are shown in Table 2.

Table 2
Crystallographic statistics for ATIC (PDB code: 7MGQ)

Diffraction data statistics	ATIC
Space group	*P 1 21 1*
Unit cell parameters a, b, c (Å); α, β, γ (°)	91.841, 115.867, 111.823; 90, 96.183, 90
Molecules per asymmetric unit	1
Resolution range (Å)	48.92–2.67 (2.77–2.67)
Unique reflections	65,095 (6258)
Completeness (%)	98.75 (95.05)
Multiplicity	2.0 (2.0)
Average I/σ(I)	12.05 (2.06)
R_{merge} [a]	0.02776 (0.2134)
R_{meas} [b]	0.03926 (0.3018)
$CC_{1/2}$ [c]	0.999
Refinement statistics	
Resolution (Å)	2.67
Reflections used in refinement	65,083 (6258)
Reflections used for R-free	1999 (192)
R_{work} [d] (%)	20.78
R_{free} (%)	23.54
No. of amino acids	605
No. of water molecules	74
Overall *B*-factor (Å^2)	69.40
RMSDs from ideal values [e]	
Bonds (Å)	0.006
Angles (°)	1.11
Ramachandran plot	
Favoured (%)	97.35
Disallowed (%)	2.61

NB: Values within parentheses indicate the highest resolution bin.
[a] $R_{merge} = \Sigma_{hkl}(\Sigma_i(|I_{hkl,I} - <I_{hkl}>|))/\Sigma_{hkl,i} <I_{hkl}>$, where $I_{hkl,i}$ is the intensity of an individual measurement of the reflection with Miller indices h, k, and l, and $<I_{hkl}>$ is the mean intensity of that reflection. Calculated for $I > -3\sigma(I)$.
[b] $R_{meas} = \Sigma hkl\{N(hkl)/[N(hkl)\text{-}1]\}\ 1/2\ \Sigma i|Ii(hkl) - <I(hkl)>|/\Sigma hkl\Sigma iIi(hkl)$, where $Ii(hkl)$ is the intensity of the *i*th measurement of an equivalent reflection with indices *hkl*.
[c] Calculated with the program Aimless.
[d] $R_{work} = \Sigma_{hkl}(||Fobs_{hkl}| - |Fcalc_{hkl}||)/|Fobs_{hkl}|$, where $|Fobs_{hkl}|$ and $|Fcalc_{hkl}|$ represent the observed and calculated structure factor amplitudes.
[e] As calculated by MolProbity.

Data availability

The atomic coordinates and structure factors (PDB code: 7MGQ) have been deposited in the PDB (https://www.rcsb.org/).

Supporting information—This article contains supporting information (Figs. S1–S5 and Tables S1–S3).

Acknowledgments—Crystallization was conducted at the University of Queensland Remote Operation Crystallization and X-ray Diffraction Facility (UQ ROCX) in the Centre for Microscopy and Microanalysis. X-ray diffraction data were collected on the MX2 beamline at the Australian Synchrotron, Victoria, Australia. We acknowledge the facilities, and the scientific and technical assistance, of the Australian Microscopy & Microanalysis Research Facility at the Centre for Microscopy and Microanalysis, The University of Queensland, and the Australian Synchrotron.

Author contributions—J. A. F. conceptualization; M. S. I. W., S. M. H. C., J. M. L. W., and A. A. B. R. methodology; U. K., B. K., and J. A. F. validation; M. S. I. W., Z. L., M. K. M., and M. P. formal analysis; M. S. I. W., S. M. H. C., and Z. L. investigation; M. S. I. W. data curation; M. S. I. W. writing–original draft; S. M. H. C., A. A. B. R., U. K., B. K., and J. A. F. writing–review & editing; M. S. I. W. and S. M. H. C. visualization; U. K., B. K., and J. A. F. supervision; M. S. I. W. project administration; J. A. F. funding acquisition.

Funding and additional information—This research was supported by the National Health and Medical Research Council (http://www.nhmrc.gov.au/; grant no.: APP1130192; to J. A. F.). B. K. is Australian Research Council Laureate Fellow (grant no.: FL180100109).

Conflict of interest—The authors declare that they have no conflicts of interest with the contents of this article.

Abbreviations—The abbreviations used are: AICAR, 5-aminoimidazole-4-carboxamide ribonucleotide; ATIC, AICAR transformylase/5′-inosine monophosphate cyclohydrolase; FAICAR, phosphoribosylformamidocarboxamide; IMP, 5′-inosine monophosphate; MALS, multiangle laser light scattering; N^{10}-fTHF, N^{10}-formyl-tetrahydrofolate; PDB, Protein Data Bank; SEC, size-exclusion chromatography; YNB, yeast nitrogen base; YPD, yeast extract–peptone–dextrose.

References

1. Romani, L. (2004) Immunity to fungal infections. *Nat. Rev. Immunol.* **4**, 11–24
2. Kathiravan, M. K., Salake, A. B., Chothe, A. S., Dudhe, P. B., Watode, R. P., Mukta, M. S., *et al.* (2012) The biology and chemistry of antifungal agents: a review. *Bioorg. Med. Chem.* **20**, 5678–5698
3. Hawksworth, D. L. (1991) The fungal dimension of biodiversity: magnitude, significance, and conservation. *Mycol. Res.* **95**, 641–655
4. Romani, L. (2011) Immunity to fungal infections. *Nat. Rev. Immunol.* **11**, 275–288
5. Pfaller, M. A., Pappas, P. G., and Wingard, J. R. (2006) Invasive fungal pathogens: current epidemiological trends. *Clin. Infect. Dis.* **43**, S3–S14
6. Caicedo, L. D., Alvarez, M. I., Delgado, M., and Cárdenas, A. (1999) *Cryptococcus neoformans* in bird excreta in the city zoo of Cali, Colombia. *Mycopathologia* **147**, 121–124
7. Irokanulo, E., Makinde, A., Akuesgi, C., and Ekwonu, M. (1997) *Cryptococcus neoformans* var neoformans isolated from droppings of captive birds in Nigeria. *J. Wildl. Dis.* **33**, 343–345
8. Refojo, N., Perrotta, D., Brudny, M., Abrantes, R., Hevia, A., and Davel, G. (2009) Isolation of *Cryptococcus neoformans* and *Cryptococcus gattii* from trunk hollows of living trees in Buenos Aires City, Argentina. *Med. Mycol.* **47**, 177–184
9. Casadevall, A., Cleare, W., Feldmesser, M., Glatman-Freedman, A., Goldman, D. L., Kozel, T. R., *et al.* (1998) Characterization of a murine monoclonal antibody to *Cryptococcus neoformans* polysaccharide that is a candidate for human therapeutic studies. *Antimicrob. Agents Chemother.* **42**, 1437–1446
10. Casadevall, A., Kwon-Chung, K. J., Perfect, J. R., Kozel, T. R., and Heitman, J. (2011) *Cryptococcus: From Human Pathogen to Model Yeast*, ASM Press, Washington, DC
11. Rajasingham, R., Smith, R. M., Park, B. J., Jarvis, J. N., Govender, N. P., Chiller, T. M., *et al.* (2017) Global burden of disease of HIV-associated cryptococcal meningitis: an updated analysis. *Lancet Infect. Dis.* **17**, 873–881
12. Stevens, D. A. (2009) Clinical aspergillosis for basic scientists. *Med. Mycol.* **47**, S1–4
13. Cheong, C.-G., Wolan, D. W., Greasley, S. E., Horton, P. A., Beardsley, G. P., and Wilson, I. A. (2004) Crystal structures of human bifunctional enzyme aminoimidazole-4-carboxamide ribonucleotide transformylase/IMP cyclohydrolase in complex with potent sulfonyl-containing antifolates. *J. Biol. Chem.* **279**, 18034–18045
14. Elion, G. B. (1989) The purine path to chemotherapy. *science* **244**, 41–47
15. Le Nours, J., Bulloch, E. M., Zhang, Z., Greenwood, D. R., Middleditch, M. J., Dickson, J. M., *et al.* (2011) Structural analyses of a purine biosynthetic enzyme from *Mycobacterium tuberculosis* reveal a novel bound nucleotide. *J. Biol. Chem.* **286**, 40706–40716
16. Hartman, S. C., and Buchanan, J. M. (1959) Nucleic acids, purines, pyrimidines (nucleotide synthesis). *Annu. Rev. Biochem.* **28**, 365–410
17. Brown, A. M., Hoopes, S. L., White, R. H., and Sarisky, C. A. (2011) Purine biosynthesis in archaea: variations on a theme. *J. Biol. Direct.* **6**, 63
18. Chapuis, A. G., Rizzardi, G. P., D'agostino, C., Attinger, A., Knabenhans, C., Fleury, S., *et al.* (2000) Effects of mycophenolic acid on human immunodeficiency virus infection *in vitro* and *in vivo*. *Nat. Med.* **6**, 762–768
19. Chua, S. M. H., and Fraser, J. A. (2020) Surveying purine biosynthesis across the domains of life unveils promising drug targets in pathogens. *Immunol. Cell Biol.* **98**, 819–831
20. Beardsley, G. P., Rayl, E. A., Gunn, K., Moroson, B. A., Seow, H., Anderson, K. S., *et al.* (1998) Structure and functional relationships in human pur H. In *Purine and Pyrimidine Metabolism in Man IX*, Springer, New York, NY: 221–226
21. Greasley, S. E., Horton, P., Ramcharan, J., Beardsley, G. P., Benkovic, S. J., and Wilson, I. A. (2001) Crystal structure of a bifunctional transformylase and cyclohydrolase enzyme in purine biosynthesis. *Nat. Struct. Biol.* **8**, 402–406
22. Reyes, V. M., Greasley, S. E., Stura, E. A., Beardsley, G. P., and Wilson, I. A. (2000) Crystallization and preliminary crystallographic investigations of avian 5-aminoimidazole-4-carboxamide ribonucleotide transformylase–inosine monophosphate cyclohydrolase expressed in *Escherichia coli*. *Acta Crystallogr. Sect. D: Biol. Crystallogr.* **56**, 1051–1054
23. Rayl, E. A., Moroson, B. A., and Beardsley, G. P. (1996) The human purH gene product, 5-aminoimidazole-4-aarboxamide ribonucleotide formyltransferase/IMP cyclohydrolase cloning, sequencing, expression, purification, kinetic analysis, and domain mapping. *J. Biol. Chem.* **271**, 2225–2233
24. Tibbetts, A. S., and Appling, D. R. (2000) Characterization of two 5-aminoimidazole-4-carboxamide ribonucleotide transformylase/inosine monophosphate cyclohydrolase isozymes from *Saccharomyces cerevisiae*. *J. Biol. Chem.* **275**, 20920–20927
25. Vázquez-Salazar, A., Becerra, A., and Lazcano, A. (2018) Evolutionary convergence in the biosyntheses of the imidazole moieties of histidine and purines. *PLoS One* **13**, e0196349
26. Hurlimann, H. C., Laloo, B., Simon-Kayser, B., Saint-Marc, C., Coulpier, F., Lemoine, S., *et al.* (2011) Physiological and toxic effects of the purine

intermediate 5-amino-4-imidazolecarboxamide ribonucleotide (AICAR) in yeast. *J. Biol. Chem.* **286**, 30994–31002
27. Malykh, E. A., Butov, I. A., Ravcheeva, A. B., Krylov, A. A., Mashko, S. V., and Stoynova, N. V. (2018) Specific features of L-histidine production by *Escherichia coli* concerned with feedback control of AICAR formation and inorganic phosphate/metal transport. *Microbial Cell Factories* **17**, 42
28. Chitty, J. L., Blake, K. L., Blundell, R. D., Koh, Y. A. E., Thompson, M., Robertson, A. A., *et al.* (2017) *Cryptococcus neoformans* ADS lyase is an enzyme essential for virulence whose crystal structure reveals features exploitable in antifungal drug design. *J. Biol. Chem.* **292**, 11829–11839
29. Weber, G. (1983) Enzymes of purine metabolism in cancer. *Clin. Biochem.* **16**, 57–63
30. Jenkins, A., Cote, C., Twenhafel, N., Merkel, T., Bozue, J., and Welkos, S. (2011) Role of purine biosynthesis in *Bacillus anthracis* pathogenesis and virulence. *Infect. Immun.* **79**, 153–166
31. Efferth, T., Gebhart, E., Ross, D. D., and Sauerbrey, A. (2003) Identification of gene expression profiles predicting tumor cell response to l-alanosine. *Biochem. Pharmacol.* **66**, 613–621
32. Morrow, C. A., Valkov, E., Stamp, A., Chow, E. W., Lee, I. R., Wronski, A., *et al.* (2012) *De novo* GTP biosynthesis is critical for virulence of the fungal pathogen *Cryptococcus neoformans*. *PLoS Pathog.* **8**, e1002957
33. Morrow, C. A., Stamp, A., Valkov, E., Kobe, B., and Fraser, J. A. (2010) Crystallization and preliminary X-ray analysis of mycophenolic acid-resistant and mycophenolic acid-sensitive forms of IMP dehydrogenase from the human fungal pathogen Cryptococcus. *Acta Crystallogr. Sect. F: Struct. Biol. Crystallization Commun.* **66**, 1104–1107
34. Blundell, R. D., Williams, S. J., Arras, S. D., Chitty, J. L., Blake, K. L., Ericsson, D. J., *et al.* (2016) Disruption of *de novo* adenosine triphosphate (ATP) biosynthesis abolishes virulence in *Cryptococcus neoformans*. *ACS Infect. Dis.* **2**, 651–663
35. Arras, S. D., Chitty, J. L., Blake, K. L., Schulz, B. L., and Fraser, J. A. (2015) A genomic safe haven for mutant complementation in *Cryptococcus neoformans*. *PLoS One* **10**, e0122916
36. Salas, S., Bennett, J., Kwon-Chung, K., Perfect, J., and Williamson, P. (1996) Effect of the laccase gene CNLAC1, on virulence of *Cryptococcus neoformans*. *J. Exp. Med.* **184**, 377–386
37. Garber, G. (2001) An overview of fungal infections. *drugs* **61**, 1–12
38. De Jesus, M., Moraes Nicola, A., Chow, S.-K., Lee, I. R., Nong, S., Specht, C. A., *et al.* (2010) Glucuronoxylomannan, galactoxylomannan, and mannoprotein occupy spatially separate and discrete regions in the capsule of *Cryptococcus neoformans*. *virulence* **1**, 500–508
39. Verma, P., Kar, B., Varshney, R., Roy, P., and Sharma, A. K. (2017) Characterization of AICAR transformylase/IMP cyclohydrolase (ATIC) from *Staphylococcus lugdunensis*. *FEBS J.* **284**, 4233–4261
40. Mueller, W. T., and Benkovic, S. J. (1981) On the purification and mechanism of action of 5-aminoimidazole-4-carboxamide-ribonucleotide transformylase from chicken liver. *Biochemistry* **20**, 337–344
41. Baggott, J. E., and Krumdieck, C. L. (1979) Folylpoly-. Gamma.-Glutamates as cosubstrates of 10-formyltetrahydrofolate: 5'-Phosphoribosyl-5-Amino-4-Imidazolecarboxamide formyltransferase. *Biochemistry* **18**, 1036–1041
42. Wolan, D. W., Cheong, C.-G., Greasley, S. E., and Wilson, I. A. (2004) Structural insights into the human and avian IMP cyclohydrolase mechanism *via* crystal structures with the bound XMP inhibitor. *Biochemistry* **43**, 1171–1183
43. Wolan, D. W., Greasley, S. E., Beardsley, G. P., and Wilson, I. A. (2002) Structural insights into the avian AICAR transformylase mechanism. *Biochemistry* **41**, 15505–15513
44. Axelrod, H. L., McMullan, D., Krishna, S. S., Miller, M. D., Elsliger, M. A., Abdubek, P., *et al.* (2008) Crystal structure of AICAR transformylase IMP cyclohydrolase (TM1249) from *Thermotoga maritima* at 1.88 A resolution. *Proteins* **71**, 1042–1049
45. Lesch, M., and Nyhan, W. L. (1964) A familial disorder of uric acid metabolism and central nervous system function. *Am. J. Med.* **36**, 561–570
46. Cardinale, D., Salo-Ahen, O. M., Ferrari, S., Ponterini, G., Cruciani, G., Carosati, E., *et al.* (2010) Homodimeric enzymes as drug targets. *Curr. Med. Chem.* **17**, 826–846
47. Asby, D. J., Cuda, F., Beyaert, M., Houghton, F. D., Cagampang, F. R., and Tavassoli, A. (2015) AMPK activation via modulation of *De novo* purine biosynthesis with an inhibitor of ATIC homodimerization. *Chem. Biol.* **22**, 838–848
48. Janbon, G., Ormerod, K. L., Paulet, D., Byrnes, E. J.,, 3rd, Yadav, V., Chatterjee, G., *et al.* (2014) Analysis of the genome and transcriptome of *Cryptococcus neoformans* var. grubii reveals complex RNA expression and microevolution leading to virulence attenuation. *PLoS Genet.* **10**, e1004261
49. Robert, X., and Gouet, P. (2014) Deciphering key features in protein structures with the new ENDscript server. *Nucleic Acids Res* **42**(Web Server issue), W320–W324
50. Fraser, J. A., Subaran, R. L., Nichols, C. B., and Heitman, J. (2003) Recapitulation of the sexual cycle of the primary fungal pathogen Cryptococcus neoformans var. gattii: implications for an outbreak on vancouver Island, Canada. *Eukaryot. Cell* **2**, 1036–1045
51. Goins, C. L., Gerik, K. J., and Lodge, J. K. (2006) Improvements to gene deletion in the fungal pathogen *Cryptococcus neoformans*: absence of Ku proteins increases homologous recombination, and co-transformation of independent DNA molecules allows rapid complementation of deletion phenotypes. *Fungal Genet. Biol.* **43**, 531–544
52. Arras, S. D., and Fraser, J. A. (2016) Chemical inhibitors of non-homologous end joining increase targeted construct integration in *Cryptococcus neoformans*. *PLoS One* **11**, e0163049
53. Stols, L., Gu, M., Dieckman, L., Raffen, R., Collart, F. R., and Donnelly, M. I. (2002) A new vector for high-throughput, ligation-independent cloning encoding a tobacco etch virus protease cleavage site. *Protein Expr. Purif.* **25**, 8–15
54. Black, S. L., Black, M. J., and Mangum, J. H. (1978) A rapid assay for 5-amino-4-imidazolecarboxamide ribotide transformylase. *Anal. Biochem.* **90**, 397–401
55. Rabinowitz, J. C. (1963) [116] Preparation and properties of 5,10-methenyltetrahydrofolic acid and 10-formultetrahydrofolic acid. In *Methods in Enzymology*, Academic Press, Cambridge, MA: 814–815
56. Lukens, L., and Flaks, J. (1963) [96] intermediates in purine nucleotide synthesis. *Met. Enzymol.* **6**, 671–702
57. Cowieson, N. P., Aragao, D., Clift, M., Ericsson, D. J., Gee, C., Harrop, S. J., *et al.* (2015) MX1: a bending-magnet crystallography beamline serving both chemical and macromolecular crystallography communities at the Australian Synchrotron. *J. Synchrotron Radiat.* **22**, 187–190
58. Kabsch, W. (2010) Xds. *Acta Crystallogr. D Biol. Crystallogr.* **66**, 125–132
59. Collaborative Computational Project, N. (1994) The CCP4 suite: programs for protein crystallography. *Acta Crystallogr. D Biol. Crystallogr.* **50**, 760–763
60. McCoy, A. J., Grosse-Kunstleve, R. W., Adams, P. D., Winn, M. D., Storoni, L. C., and Read, R. J. (2007) Phaser crystallographic software. *J. Appl. Crystallogr.* **40**, 658–674
61. Terwilliger, T. C., Grosse-Kunstleve, R. W., Afonine, P. V., Moriarty, N. W., Zwart, P. H., Hung, L. W., *et al.* (2008) Iterative model building, structure refinement and density modification with the PHENIX AutoBuild wizard. *Acta Crystallogr. D Biol. Crystallogr.* **64**, 61–69
62. Emsley, P., Lohkamp, B., Scott, W. G., and Cowtan, K. (2010) Features and development of Coot. *Acta Crystallogr. D Biol. Crystallogr.* **66**, 486–501